



1 **ASSESSING THE PEATLAND HUMMOCK-HOLLOW CLASSIFICATION**
2 **FRAMEWORK USING HIGH-RESOLUTION ELEVATION MODELS: IMPLICATIONS**
3 **FOR APPROPRIATE COMPLEXITY ECOSYSTEM MODELLING**

4

5 Paul A. Moore^{1*}, Maxwell C. Lukenbach¹, Dan K. Thompson², Nick Kettridge³, Gustaf
6 Granath⁴, and James M. Waddington¹

7

8 ¹ School of Geography and Earth Sciences, McMaster University, 1280 Main Street West,
9 Hamilton, ON, L8S 4K1, Canada

10 ² Northern Forestry Centre, Canadian Forest Service, Natural Resources Canada,
11 Edmonton, Alberta, AB, T6H 3S5, Canada

12 ³ School of Geography, Earth and Environmental Sciences, University of Birmingham,
13 Edgbaston, Birmingham, B15 2TT, United Kingdom.

14 ⁴ Department of Ecology and Genetics, Uppsala University, Norbyvägen 18D, 736 52
15 Uppsala, Sweden

16

17 * Corresponding author: Paul Moore (paul.moore82@gmail.com)

18 Manuscript for submission to Biogeosciences

19

20 **KEY WORDS:** peatland, microtopography, morphometry, hummock, hollow, sampling

21 design, ecosystem modelling, digital elevation model



22 **ABSTRACT**

23 The hummock-hollow classification framework used to categorize peatland ecosystem
24 microtopography is pervasive throughout peatland experimental designs and current
25 peatland ecosystem modelling approaches. However, identifying what constitutes a
26 representative hummock-hollow pair within a site and characterizing hummock-hollow
27 variability within or between peatlands remains largely unassessed. Using structure-
28 from-motion (SfM), high resolution digital elevation models (DEM) of hummock-hollow
29 microtopography were used to: 1) examined how much area needs to be sampled to
30 characterize site-level microtopographic variation; and 2) examine the potential role of
31 microtopographic shape/structure on biogeochemical fluxes using data from 9 norther
32 peatlands. To capture 95% of site-level microtopographic variability, on average an
33 aggregate sampling area of 32 m² composed of ten randomly located plots with
34 vegetation removed was required. We further present non-destructive transect-based
35 results as an alternative to the SfM approach. Microtopography at the plot-level was
36 often found to be non-bimodal, as assessed using a Gaussian mixture model (GMM).
37 Our findings suggest that the non-bimodal distribution of microtopography at the plot-
38 level may result in an under-sampling of intermediate topographic position. Extended to
39 the modelling domain, an under-representation of intermediate microtopographic
40 positions is shown to lead to large flux biases over a wide range of water table positions
41 for ecosystem processes which are non-linearly related to water and energy availability
42 at the moss surface. A range of tools examined herein can be used to easily
43 parameterize peatland models, from GMMs used as simple transfer functions, to
44 spatially explicit fractal landscapes based on simple power law relations between



45 microtopographic variability and scale.

46

47 INTRODUCTION

48 Northern peatlands in the maritime-temperate, boreal, and subarctic have been
49 persistent terrestrial sinks for carbon throughout the Holocene, storing approximately
50 one-third of all global soil carbon (Yu, 2012). However, these peatland carbon stores
51 are now considered to be at risk from the effects of climate change due to warmer
52 temperatures and prolonged periods of drought which would increase carbon loss
53 through decomposition and increased wildfire consumption (Moore et al., 1998; Yu et al.,
54 2009; Turetsky et al., 2002; Kettridge et al., 2015). While these positive feedbacks
55 cause carbon loss (e.g. Ise et al., 2008; Blodau et al., 2004), the long-term stability of
56 peatland carbon may be maintained by negative ecohydrological feedbacks that
57 promote resilience to environmental change (Belyea and Clymo, 2001; Waddington et
58 al., 2015; Hodgkins et al., 2018). These negative feedbacks depend, in part, on the
59 presence of microtopography (microforms) that provides spatial diversity in
60 ecohydrological structure and biogeochemical function across a peatland (Belyea and
61 Clymo, 2001; Belyea and Malmer, 2004; Eppinga et al., 2008; Pedrotti et al., 2014;
62 Malhotra et al., 2016).

63

64 Peatland microform classification is typically defined by their proximity to the water table
65 and characteristic vegetation assemblages, such as different species of *Sphagnum*
66 moss and cover of woody shrubs (Andrus et al., 1983; Rydin and McDonald, 1985;
67 Belyea and Clymo, 1998). Hummocks and hollows occur at a spatial scale of 1 to 10 m



68 (S2 – Belyea and Baird, 2006), with the surface of hummocks usually covering an area
69 on the order of 1 m². The hummock surface is typically located ~0.20 m or higher above
70 the water table (Belyea and Clymo 1998; Malhotra et al., 2016). Hollows are closer to
71 the water table and may occasionally be inundated, and ‘lawns’ are intermediate to
72 hummocks and hollows (Belyea and Clymo, 1998).

73

74 Conceptualizing and qualitatively classifying complex peatland microtopography as
75 hummocks and hollows is common in peatland research (e.g. Waddington and Roulet
76 1996; Belyea and Clymo 2001; Nungesser 2003; Benscoter et al., 2005; Bruland and
77 Richardson 2005; Moser et al., 2007) as it is simple and allows for straightforward
78 sampling designs, however, the visual characterization of hummocks and hollows is
79 subjective and has the potential to produce biased results for several reasons. First,
80 although microform vegetation and hydrology may be included in detailed study
81 site/method descriptions, these characteristics may be quite different for microforms
82 classified as hummocks at one study site compared to hummocks at a different study
83 site. Biogeochemical function (ecosystem fluxes) may differ for microforms within a site
84 (e.g. Bubier et al., 1993; Pelletier et al., 2011), but if the vegetation and hydrology of
85 those microforms vary for different peatlands, assumptions for hummock and hollow
86 biogeochemical function at one site may not be applicable to other peatlands. Given
87 that there may also be large differences in the relative/absolute height and surface
88 roughness of microforms between sites, comparing studies with hummock and hollow
89 microforms as a central component of the sampling design can be problematic.
90 Moreover, the surface area, spatial distribution, and relative proportion of hummock and



91 hollow microforms present within a peatland also vary between sites (e.g. Moore et al.,
92 2015), which may introduce bias into sampling design. For example, researchers may
93 over-sample the visually obvious extremes of the hummock-hollow continuum. Given
94 that several peatland hydrological and ecosystem carbon models parameterize peat
95 decomposition, production and hydraulic properties based on peatland microform
96 classification (e.g. Dimitrov et al., 2010; Sonnentag et al., 2008), the aforementioned
97 sampling and classification biases may also lead to issues in determining the scale and
98 complexity required for ecosystem modelling (e.g. Larsen et al., 2016).

99

100 The construction of a digital elevation model (DEM) in a peatland allows for the
101 classification of microforms based on quantitative measures (e.g. relative position, slope,
102 or roughness) (e.g. Mercer and Westbrook, 2016; Rahman et al., 2017) rather than
103 relying on qualitative/visual methods. Given the wide use and adoption of the hummock-
104 hollow conceptual framework, we examine the potential utility of DEM quantitative
105 techniques to overcome the concerns with the dominant qualitative hummock and
106 hollow framework/classification scheme. As such, the two main objectives of this study
107 were to: (i) provide a geostatistical/geospatial description of plot scale microtopographic
108 variation in peatlands; and (ii) to use simple physically-based and empirical models to
109 examine the effect of measured microtopographic complexity on ecosystem fluxes. For
110 the first objective, our two main focuses were: i) using a case-study approach, assess
111 how much area needs to be sampled in order to be able to adequately quantify
112 microtopographic variability within an unpatterned peatland; and ii) using multi-site plot-
113 scale sampling, explore DEM-derived morphometric properties (e.g. microtopography



114 height distribution, slope, and roughness) of peatland microforms which may be useful
115 as microtopographic metrics.

116

117 **METHODS**

118 ***Experimental design***

119 We first evaluated how much sampling area is needed to capture the overall
120 microtopographic variation of an unpatterned site using both structure-from-motion (SfM)
121 (see Brown and Lowe 2005; Mercer and Westbrook 2016) and a transect based
122 sampling approach. To accomplish this, we randomly sampled 50 plots for SfM
123 reconstruction in a peatland near Red Earth Creek, AB (56.54°N 115.22°W) (hereafter
124 referred to as site-level). In addition, we manually measured surface elevation along
125 several 50 m transects at 0.05 m intervals covering the plot area at the Red Earth Creek
126 site. Secondly, we used SfM to examine morphometric properties at the plot scale in 9
127 boreal/hemi-boreal, non-permafrost, ombrotrophic peatlands (4 in Canada, 4 in USA, 1
128 in Sweden; see Table 1) using two different approaches. The first approach involved
129 randomly selecting 9 plot locations within a single site and creating a plot around the
130 random location which was perceived to contain a hummock-hollow pair. The second
131 approach involved qualitatively choosing what was perceived to be a representative
132 hummock-hollow pair at 9 different sites. The aim of our approach was to highlight the
133 potential breadth of variation in morphometric properties which might be observed either
134 within a site (*i.e.* implications for small sample size) or across sites (*i.e.* highlight
135 potential challenges with site inter-comparisons without supporting information of
136 peatland microtopographic metrics). For both randomly located plots and qualitatively



137 chosen plots, individuals were asked to identify a central point for a hummock and
138 hollow subplot within the larger microtopography plot.

139 ***Site preparation and image acquisition protocol***

140 All vascular vegetation was removed from the plot area using scissors and hand
141 pruners in order to provide an unobstructed view of the surface microtopographic
142 variation (moss surface) for imaging. Matte-colored discs ($n=20$) of 0.04 m diameter
143 were placed randomly on the clipped surface to provide reference points for better
144 correlation between images. To provide absolute scale and orientation, two boxes of
145 known dimensions (0.1×0.1×0.1 m) were placed in each plot and levelled prior to image
146 acquisition. Images of each target area were taken via at least two circuits around the
147 plot, with images taken from two separate vertical viewing angles (see
148 http://www.cs.cmu.edu/~reconstruction/basic_workflow.html for third party description of
149 general workflow). Distance to target area was set so that a large portion of the clipped
150 area was visible in each image. To produce different horizontal viewing angles, images
151 were taken every one or two paces around the perimeter of the plot. This procedure
152 yielded 41 to 282 overlapping images from multiple view-points of the plot areas, which
153 ranged in size from 3.2 to 10.1 m² (Table 1). Images were taken during either clear-sky
154 or over-cast conditions near mid-day during the summer to avoid changing lighting
155 conditions and to limit self-shadowing of the surface. Images were captured with digital
156 cameras using automatic exposure settings. Prior to analysis, all images were
157 downsampled where necessary to a common resolution of 2048 x 1536 using a Lanczos3
158 filter.

159



160 ***Digital elevation models of microtopography***

161 A point-cloud of the moss surface was generated using an SfM approach (Brown and
162 Lowe 2005; Mercer and Westbrook 2016) using the program Visual SfM (Wu, 2011).
163 Visual SfM identifies image features for cross-comparison using a scale-invariant
164 feature transform (Lowe, 1999), and then matches features between images in a
165 pairwise manner. Effectively, this creates multiple stereo-pairs from which camera
166 position and scene geometry can be estimated through triangulation. This procedure
167 yielded average point cloud densities ranging from 3-59 pixels cm⁻² for the imaged plots
168 (Table 1).

169

170 Prior to generating the DEMs, point clouds were cropped to the region of interest (*i.e.*
171 area of clipped vegetation), then scaled, levelled, and oriented using the rendered
172 reference objects. DEMs were produced using the MATLAB function *TriScatteredInterp*
173 (MATLAB R2010a, The Mathworks), which performs Delaunay triangulation of the point
174 clouds. DEMs were generated on a 0.01 x 0.01 m grid using natural neighbor (Voronoi)
175 interpolation. The DEMs were smoothed using a mean filter window with a size of 0.03 x
176 0.03 m. Finally, a mask was applied to the DEMs to remove reference objects.

177

178 ***Capturing site-level microtopographic variation***

179 Plots from the Red Earth Creek peatland were ~3.5 m² and differences between plot
180 elevation for the 50 plots were surveyed using a Smart Leveler digital water level
181 (accuracy ±2.5 mm), with offsets applied to DEMs. A Monte Carlo re-sampling approach
182 was used to evaluate how total variance in microtopographic elevation increased with



183 increasing sample size. For each sample size (*i.e.* 1-50), 200 random re-samplings
184 were performed. To estimate the change in variance with increasing sample size, a
185 rectangular hyperbola was fit to the mean variance (y) versus sample size (x):

$$186 \quad y = \frac{ax+b-\sqrt{(ax+b)^2-4axbc}}{2c}$$

187 where b is the estimated maximum total variance, and a and c are initial slope and
188 concavity parameters.

189

190 To evaluate the dominant scale of microtopographic variation which contributes to total
191 variance, a fast Fourier transform (*fft* function in MATLAB) was used to estimate the
192 power spectral density (PSD) of microtopographic variation along an artificially
193 constructed 300 m long transect (combination of multiple transects). Manual
194 measurements of moss surface elevation were taken every 0.05 m along six 50 m
195 transects at the Red Earth Creek, AB and Nobel, ON site using the Smart Leveler.

196

197 ***Plot-level microtopographic variation***

198 Plot-level microtopographic variation was analyzed using randomly and qualitatively
199 chosen plot locations listed in Table 1. Based on the hummock-hollow conceptual model,
200 our *a priori* assumption was that a hummock-hollow pair would have a bi-modal
201 distribution of surface elevation. Our null hypothesis was that microtopography would
202 follow a bi-modal distribution, so we evaluated DEM height distributions using 1– to 3–
203 member Gaussian mixture models (GMM) to evaluate whether 2-member GMMs would
204 best explain height distributions. GMMs were fit to DEM height distributions using the
205 MATLAB function *gmmdistribution.fit*, which uses an iterative expectation maximization



206 algorithm to determine GMM parameters representing maximum likelihood estimates.
207 The GMM fit function was seeded with initial parameter estimates using k -means
208 cluster analysis. The best model was decided based on the minimum Akaike
209 information criteria (AIC).

210

211 Surface slope and aspect were evaluated using the computed surface normals for each
212 point and eight connected neighbours of the DEM. The fractal dimension of plots was
213 evaluated using radially averaged PSD derived from an fft of elevation data. The Hurst
214 (H) exponent (values of 0–1) presented herein is related to fractal dimension as $3-H$,
215 where the slope of the PSD curve in log space is $-2(H+1)$.

216

217 ***Modelled moss surface insolation and productivity***

218 Potential moss surface insolation was modelled using the formulation presented in
219 Kumar et al. (1997) to account for earth-sun geometry, surface slope and aspect, and
220 diffuse radiation under clear-sky conditions. Total potential insolation was evaluated on
221 an annual basis and normalized relative to total insolation on a flat surface for each plot
222 location.

223

224 For moss net primary productivity (NPP) and capitula water content (WC), each plot
225 was classified into three units based on relative elevation which notionally correspond
226 with hollow/lawn, low hummock, high hummock. K-means clustering was used to
227 perform unsupervised classification of microtopographic elevation (Figure S1). A
228 separate parameterization for moss NPP and WC was used for each elevation cluster.



229 Parameterizations for hollow/lawn, low hummock, and high hummock were obtained
230 from *Sphagnum* species of the section Cuspidata, *Sphagnum*, and *Acutifolia*,
231 respectively (Figure S2). An empirical relation between WC and water table depth (WTD)
232 was modelled as follows:

$$233 \quad WC = p_1 \cdot \ln(p_2 \cdot WTD) + p_3$$

234 where WC is in $\text{g}_{\text{water}} \text{g}_{\text{dry weight}}^{-1}$, and p_{1-3} are fitted parameters. WC was restricted to a
235 range of 1–25 $\text{g}_{\text{water}} \text{g}_{\text{dry weight}}^{-1}$. A rational function was used to model the relation
236 between moss capitula NPP and WC:

$$237 \quad NPP_{pot} = 100 \cdot \left(\frac{p_4 \cdot x^2 + p_5 \cdot x + p_6}{x^2 + p_7 \cdot x + p_8} \right) \cdot NPP_{max}^{-1}$$

238 where NPP_{pot} represents % of maximum NPP, and p_{4-8} are fitted parameters. Estimates
239 of 83, 170, and 198 $\text{g m}^{-2} \text{mo}^{-1}$ for NPP_{max} were used to represent *Sphagnum* species of
240 section Cuspidata, *Sphagnum*, and *Acutifolia*, respectively (Nungesser, 2003).

241

242

243 RESULTS

244 *Site-level microtopographic variation*

245 In characterizing microtopographic variability across the Red Earth Creek site, our data
246 shows that variability in surface elevation increases asymptotically with sample size (*i.e.*
247 area sampled) and is well predicted by a rectangular hyperbola ($r^2=0.98$; $p<<0.01$) (Fig.
248 1). Based on the asymptote of the fitted rectangular hyperbola (0.147 m), Figure 1
249 shows that on average an area of 32 m^2 (*i.e.* 9 random plots of $\sim 3.5 \text{ m}^2$ size) contains
250 roughly 95% of the predicted site-scale microtopographic variability. Even though
251 increasing the number of plots by a factor of 5 (*i.e.* ~ 50 plots) has little effect on the



252 average variance in surface elevation, the range associated with re-sampling is reduced
253 by about half (Fig. 1 – shaded area).

254

255 While the Red Earth Creek multi-plot DEM data provides the ability to assess the area
256 required to capture site-scale microtopographic variability for a small unpatterned
257 Alberta peatland, it does not directly provide information on what spatial scales
258 contribute most to overall variability. The power spectral density (PSD) of manual
259 elevation transects from both the Red Earth Creek and Nobel sites suggests that most
260 of the microtopographic variation for these two surveyed sites occurs at spatial scales
261 between 1–10 m (Fig. 2 – cumulative curves). Both sites have qualitatively similar PSD
262 curves in log-space with a roll-off at spatial scales between 2.6–3.1 m (break point of
263 piecewise regression). Moreover, the PSD of microtopographic variation appears to be
264 well described by a power law (*i.e.* relatively smooth slope in log space) at small spatial
265 scales resulting in a Hurst exponent (see Methods for relation to fractal dimension)
266 between 0.61–0.79.

267

268 ***Plot-level hypsometry and fractal dimension***

269 There is a characteristic difference in the elevation distribution of whole-plots compared
270 to that of the corresponding hummock-hollow subplots for both qualitatively (Fig. 3) and
271 randomly (Fig. 4) chosen plot locations. The elevation distributions for hummock-hollow
272 subplots tend to have a clear separation of modes (Fig. 3-4 B-panels). The degree of
273 separation in modes has a weak ($r^2 = 0.31$) but significant linear relation ($F_{16} = 7.1$, $p =$
274 0.017) with the microtopographic range in the whole plot. On average, the elevation



275 range absent from the hummock-hollow subplots represents roughly 25% of the
276 microtopographic range of the whole plot. When all hummock-hollow subplots are
277 aggregated across randomly selected plots (*i.e.* Nobel, ON site), the whole elevation
278 distribution is captured (Fig. S3). However, there remains a bias towards higher
279 elevations being sampled in the aggregated subplot elevation distribution compared to
280 the aggregated whole plot elevation distribution.

281

282 In testing the null hypothesis of bimodally distributed relative surface elevation at the
283 plot scale, we examined the goodness of fit of one-, two-, and three-member GMMs. An
284 assessment of all 18 plots suggests that two- or three-member GMMs tend to provide a
285 better fit to reconstructed elevation distributions compared to a one-member (*i.e.* normal)
286 distribution. Based on AIC values, the one-member GMM was best for only 3 plots,
287 while two- and three-member GMMs were best for 6 and 9 plots, respectively (Table 2).
288 In contrast, when GMMs were fit to hummock-hollow subplot data, the two-member
289 GMM tended to outperform one- and three-member GMMs.

290

291 The mean (μ) and standard deviation of elevation for hummock and hollow subplots
292 were grouped and compared according to plot selection method (*i.e.* random within site
293 versus qualitative between site selection). Since the μ parameter corresponds with
294 relative elevation, we took the difference between the two members (*i.e.* $\mu_{hum} - \mu_{hol}$) for
295 comparison purposes. Overall, the qualitatively chosen plots appear to have similar
296 ($F_{1,16}=0.2$; $p=0.68$) relative hummock heights ($\mu_{hum} - \mu_{hol}$) (0.21 ± 0.08 m) compared to the
297 randomly chosen plots. (0.19 ± 0.09 m). Variation in elevation tended to be lower in



298 hollow subplots (0.032 ± 0.012 m) compared to hummock subplots (0.022 ± 0.009 m)
299 (microform; $F_{1,32}=9.0$, $p=0.005$), where the difference between hummock and hollow
300 subplots was similar when comparing qualitatively and randomly chosen sites
301 (microform \times plot type; $F_{1,32}=0.02$; $p=0.89$).

302

303 Depending on the underlying structure of spatial variability, surface roughness can be
304 highly dependent on the scale of analysis. A two-dimensional power spectral density of
305 elevation provides a means to formally describe the change in roughness with scale
306 (Fig. 5). The power spectral density of elevation was found to be a linear function of
307 length-scale across the 0.05–1 m range in log–log space ($r^2_{\text{adj}}>0.96$) and is the basis for
308 the Hurst exponent (H) (see methods for relation to fractal dimension). While the
309 distribution of H for qualitatively chosen plots (0.73 ± 0.18) was higher compared to
310 randomly chosen plots (0.60 ± 0.11) (*i.e.* comparatively less ‘complexity’ at finer spatial
311 scales), the difference was not strongly significant ($F_{1,16} = 3.63$; $p = 0.075$).

312

313 ***Plot-level slope, aspect and solar insolation***

314 A Weibull distribution provided a good fit to the slopes for the reconstructed DEMs (Fig.
315 S4), where the average, maximum, and minimum RMSE were 0.10%, 0.14%, and
316 0.06%, respectively, based on a relative frequency distribution with 1° bin sizes. When
317 grouped according to qualitatively versus randomly chosen plots, the modal slope for
318 whole plots was $21.5\pm 4.4^\circ$ and $23.4\pm 5.7^\circ$, respectively. Similarly, the distribution of
319 standard deviation in slope for randomly and qualitatively chosen plots was $14.6\pm 1.3^\circ$
320 and $14.5\pm 2.1^\circ$, respectively. Comparing the parameter distributions from the Weibull fit



321 for qualitatively and randomly chosen plots, it was found that there was no significant
322 difference in the mean scale (analogous to mode) and shape (analogous to standard
323 deviation) parameters (scale: $p=0.44$, $F_{1,16}=0.62$; shape: $p=0.88$, $F_{1,16}=0.02$).

324

325 While modal slope tended to only be slightly higher in the hummock subplots
326 ($22.9\pm 6.8^\circ$) versus hollow subplots ($19.5\pm 6.0^\circ$), there was greater distinction in the
327 prevalence of steep slopes (*i.e.* $>45^\circ$) in hummock subplots ($14.8\pm 10.4\%$) versus hollow
328 subplots ($8.4\pm 9.5\%$) (Fig. S5). Comparing slope in the hummock/hollow subplots to the
329 3-member GMM clusters (high, intermediate, and low elevations – for example see Fig.
330 S1), we see that the subplots tend to be somewhat flatter compared to the rest of the
331 plot, particularly for hollow subplots (Fig. S5).

332

333 Figure 7 shows how slope and aspect affect potential solar insolation at the moss
334 surface under ideal conditions (*i.e.* clear-sky, sparse vegetation). Potential solar
335 insolation is significantly affected by aspect ($F_{7,60820} \geq 290.8$, $p < 0.01$) and its interaction
336 with slope ($F_{7,45606} \geq 7043.7$, $p < 0.01$), where on average, south facing slopes receive
337 double the potential solar insolation compared to north facing slopes. Based on
338 measured slope and aspect at randomly and qualitatively chosen plots, median
339 potential solar insolation for a south aspect is 12-24% greater compared to a flat
340 surface. Similarly, for a north-facing aspect, median potential solar insolation is 18-40%
341 lower (Figure S6).

342



343 ***Plot-level empirical model of moss productivity using high resolution DEMs***

344 Assuming a flat water table at the plot-level, Figure 8 shows how modelled NPP_{pot}
345 varies with WTD relative to the average hollow surface. Hollows tend to have a
346 comparatively narrow range of WTD (i.e. 0–0.15 m) over which the moss is expected to
347 be highly productive compared to hummocks. Despite using species-dependent NPP_{pot} -
348 WC relations, the large differences in water table range over which hummock and
349 hollow NPP_{pot} is high is largely driven by the WC-WTD relations (Figure S2). Where
350 moss species have large differences in NPP_{max} and different characteristic water
351 retention, NPP_{pot} rarely overlaps between microtopographic classes (Figure 8). If we
352 ignore the effect of species-dependent characteristics (i.e. NPP_{max} , NPP_{pot} -WC, and
353 WC-WTD) and use a single average parameterization, differences between
354 microtopographic classes tend to be smaller for shallow water table conditions (Figure
355 S7), yet there remains a characteristic difference in mean NPP_{pot} between
356 microtopographic classes.

357

358 From a scaling perspective, modelled NPP_{pot} (Figure 8 and S7) were used to compare
359 spatially explicit estimates with plot averages based on the notional chamber subplot
360 (i.e. pre-determined 0.37 m² area in perceived hummock and hollow — see methods).
361 In general, spatially explicit NPP_{pot} estimates tended to be higher/lower than the
362 hummock-hollow estimates depending on whether the water table was relatively
363 shallow/deep (Figure 9a). The maximum positive bias between the spatially explicit and
364 hummock-hollow NPP_{pot} values ranged from 21.1–40.1 g m⁻² mo⁻¹, while the negative
365 bias ranged from -5.9 to -40.9 g m⁻² mo⁻¹. Using a single average parameterization for



366 NPP_{pot} tends to result overwhelmingly in positive bias between the spatially explicit and
367 hummock-hollow models, where maximum bias ranges from 22.7 to 58.9 g m⁻² mo⁻¹.
368 Averaged across all 18 plots, the subjective hummock subplot broadly overlapped with
369 the k-means high-hummock classification (94%), with only small portions overlapping
370 with the low-hummock classification (6%). Similarly, the subjective hollow subplot
371 broadly overlapped with the k-means hollow/lawn classification (79%), with only small
372 portions overlapping with the low-hummock classification (20%). In this study, our
373 results indicate that the subjective choice of hummock and hollow subplot location (e.g.
374 for chamber flux measurement) systematically under samples intermediate topographic
375 positions. This is exemplified in Figure S8 which shows the spatial distribution of NPP_{pot}
376 for one of the plots. For the NPP_{pot} model using separate parameterization for the
377 microtopography classes, the low-hummock class remains distinct from both the
378 hollow/lawn and high-hummock class except under very dry conditions. For the uniform
379 parameterization, the low-hummock classification is distinct from the other two classes
380 under wet conditions, behaves like the hollow/lawn under moderately dry conditions,
381 and behaves like a hummock under very dry conditions.

382

383

384 **DISCUSSION**

385 ***Assessing microform representativeness***

386 In studies which use the hummock-hollow microtopography classification as part of their
387 sampling design, there are many cases in which the plot choice is said to be
388 representative (e.g. Kettridge and Baird 2008; Laing et al., 2008; Nijp et al., 2014), but



389 often lacks detail on how representativeness was assessed. For example, when
390 characterizing the surface within an eddy covariance flux measurement footprint, it is
391 common to only sample one or few hummock-hollow pair(s) (e.g. Lafleur et al., 2003;
392 Humphreys et al., 2006; Peichl et al., 2014; Moore et al., 2015). Similarly, for direct
393 measurements of surface fluxes where microtopography is considered explicitly,
394 chamber-based measurements typically use between four and eight replicates (e.g.
395 Frenzel and Karofeld 2000; Turetsky et al., 2002; Forbrich et al., 2011; Petrone et al.,
396 2011) per microtopographic unit. For peatland studies which use random plots, as many
397 as 30 plots per site have been reported (i.e. Wieder et al., 2009), yet earlier studies
398 have reported using as few as one to four plots to characterize a site (e.g. Crill et al.,
399 1988; Shannon and White 1994; Regina et al., 1996). Using the Red Earth Creek
400 results as a reference, for studies which have 4-8 replicates, 2-3 microtopographic units
401 (e.g. hummock, lawn, hollow), and the more common chamber size of roughly 0.6 x 0.6
402 m, we would infer from our results that the typical total sample area for chamber flux
403 measurements in a peatland ecosystem would capture on the order of 70-86% of site-
404 scale microtopographic variability in their plots. It should be noted however that the
405 simple assessment above assumes that chamber placement is random. In cases with
406 lower replication of two microtopographic units, our results suggest that the uncertainty
407 associated with repeated sampling is relatively high (Fig. 1 – shaded area) and that the
408 choice of two microtopographic units could lead to an under-sampling of intermediate
409 topographic positions (e.g. Fig. 3-4 B-panels). When the ecosystem processes of
410 interest are not measured across the range of variability observed at the site-scale,
411 particularly for non-linear processes, then scaling from process-based, or simply plot-



412 scale measurements, is at risk of being biased. Our simple empirical model of moss
413 NPP_{pot} demonstrates that flux bias can be large relative to NPP_{max} and is strongly
414 dependent on water table depth (Figure 9). Although NPP_{pot} estimates are strongly
415 influenced by the parameterization used (e.g. Figure 8 and S7), there remains a large
416 bias between the spatially explicit and hummock-hollow NPP_{pot} models.

417

418 To upscale models or plot-scale measurements it is important to determine the
419 microtopographic structure and variability of a peatland. There were often non-bimodal
420 distributions of microtopography in our study sites (Fig. 3–4 A-panels and Table 2)
421 where the more continuous distribution of elevation at the plot scale suggests that when
422 experimental designs use hummock-hollow pairs as the primary experimental unit (Fig.
423 3–4 B-panels) they have a tendency to capture the ends of the distribution, omitting on
424 average 25% of the elevation distribution at the plot scale (see also Figure S3). In this
425 study we clipped vegetation in 50 small random plots to produce very high resolution
426 DEMs for assessing microtope-scale (*i.e.* S3 hummock-hollow complex, *cf.* Belyea and
427 Baird, 2006) variability, yet surface vegetation removal will generally be undesirable.
428 Ground- or drone-based SfM approaches have been used to produce a digital surface
429 model (DSM – vegetation present) for alpine (Mercer and Westbrook, 2016) and blanket
430 (Harris and Baird, 2018) peatlands with reasonable accuracy (e.g. mean absolute error
431 of ~ 0.08 m, and normalized median absolute deviation of ~ 0.11 m for the alpine and
432 blanket peatlands, respectively). In situations where surface vegetation removal is not
433 possible or desirable and/or where drone-based imagery is hampered (e.g. treed
434 peatlands), a survey of height distribution along one or several transects would provide



435 an alternative to assessing microtopo to mesotopo-scale (S3–S4 Belyea and Baird,
436 2006) microtopographic variability. The power spectral density of transect data would
437 suggest that, for absolute height, a sampling interval of less than 1 m (e.g. 0.5 m) for
438 several 50 m transects would capture the scales of variability which contribute most to
439 total height variance (Fig. 2 and 5) since this corresponds to ~90% of measured
440 microtopographic variation and provide sufficient fine-scale data to estimate the fractal
441 dimension of microtopography. Information on height distributions could provide the
442 basis for plot selection, where plots could be chosen to deliberately span the range of
443 variability, or to avoid oversampling extremes. Information on the height distribution
444 would furthermore provide the ability to scale up findings from the plot level given their
445 relative position in the wider distribution of microtopographic variability (*cf. Griffis et al.,*
446 2000).

447

448 Despite the variety of site characteristics observed, our plots were limited to bogs and
449 poor fens, and did not include sites with ridge and pool patterning. Nevertheless, our
450 results would suggest that generalizations based on a hummock-hollow classification,
451 either to the site-scale, or to hummocks-hollow pairs across sites should be viewed with
452 a degree of skepticism when sample size is low, or when a general microtopographic
453 survey is absent/unreported. Thus, for wider inter-comparability of peatland studies, SfM
454 or transect-based approaches of measuring and reporting on one or several
455 morphometric properties of microtopography could provide a more comprehensive
456 dataset to aid in future meta-analysis/synthesis.

457



458 ***Implications for appropriate complexity ecosystem modelling in peatlands***

459 The complex shape/structure of peatland microtopography has generally been ignored
460 from a modelling standpoint, but several studies have shown, for example, that slope
461 and aspect may affect peat temperature (Kettridge and Baird 2010). Under clear-sky
462 conditions, modelled annual total solar insolation differs from a flat surface by roughly
463 $\pm 20\%$ in our measured plots, where our study sites span 43° to 60°N latitude (Figure
464 S6). For north and south facing slopes, this effect is amplified (Figure 7) particularly for
465 high- and low-hummock microtopographic classes (e.g. Figure S1) which tend to have
466 greater average slope compared to the hollow/lawn classification (Figure S5). While our
467 study sites are limited to the non-permafrost boreal region, the applicability of slope and
468 aspect considerations to modelling tundra tussocks in arctic and permafrost regions is
469 also relevant (e.g. De Baets et al., 2016). Based on the results of empirical studies, the
470 shape of microtopographic features ought to play a role in ecosystem fluxes due to the
471 effect of shortwave radiation on surface evaporation (Kettridge and Baird, 2010),
472 photosynthetically active radiation on moss production (Harley et al., 1989; Loisel et al.,
473 2012), and soil temperature on methane production and respiration (e.g. Lafleur et al.,
474 2005; Waddington et al., 2009). It is important to note, however, that under cloudy
475 conditions the increasing proportion of total insolation from diffuse radiation decreases
476 the disparity in insolation associated with slope and aspect. Furthermore, in peatlands
477 where substantial tree, shrub, or graminoid cover exists, the importance of slope and
478 aspect on soil heating or ecosystem fluxes is likely to be low since insolation decreases
479 exponentially with increasing vascular leaf area.

480



481 In addition to microtopographic shape/structure, the size of microtopographic features
482 and their small-scale variability can similarly affect ecosystem fluxes, where height
483 above water table imposes a first order control on water availability. Methane fluxes
484 from peatlands, for example, have been shown to vary logarithmically over 0.1 m scales
485 (Turetsky, 2014). Water availability at the moss surface has been shown to be both
486 species-dependent and strongly affected by water table (Hayward and Clymo, 1982;
487 Rydin, 1985), where moss species and water availability has been linked to many
488 ecohydrological processes such as surface evaporation (Kettridge and Waddington,
489 2014), productivity (Williams and Flanagan, 1998; Strack and Price, 2009), and
490 hydrophobicity (Moore et al., 2017). We show that when microtopographic variability is
491 explicitly modelled, complex patterns of potential moss productivity emerge (Figure S8)
492 which are not captured by a hummock-hollow model (Figure 9), and that the presence
493 of bias is independent of whether moss species niche partitioning is considered.

494

495 The SfM method is a potentially useful tool for examining both how morphometric
496 properties of the surface which affect ecohydrological processes vary within a site.
497 Moreover, information on microtopographic variability and structure from SfM-derived
498 DEMs can be used to further examine the potential role of fine-scale microtopographic
499 variability on biogeochemical processes within a modelling domain. The GMM is a
500 simple way to include a more realistic description of height distributions within
501 distributed peatland models (e.g. Dimitrov et al., 2010), or extend from the meso- to
502 micro-scale (Sonnentag et al., 2008). Computationally, GMMs are a relatively efficient
503 way of representing microtopographic variability, needing only two parameters per



504 member of the GMM distribution. Conceptually, the GMM distribution can be applied
505 directly in distributed peatland models to populate relative heights of individual cells. In
506 the case of one-dimensional models, a GMM distribution can be used as a transfer
507 function for any water table dependent processes, particularly in cases where the
508 relation is non-linear. Alternatively, a small number of parameters from the PSD of
509 microtopographic elevation (e.g. variance, Hurst exponent, and spatial scale of break
510 point), be it from a DEM (Fig. S4) or transect (Fig. 2), can be used to generate ‘synthetic’
511 microtopography which includes spatial structure in elevation change rather than just
512 the distribution.

513

514 **CONCLUSIONS**

515 The magnitude of variation in assessed morphometric properties within a site (randomly
516 chosen plots) is commensurate with the range across sites (qualitative plots) where
517 mean differences are comparatively small. With a small effect size, our results highlight
518 the need for adequate spatial sampling in process-based studies of microform function,
519 particularly when upscaling to the whole peatland or in order to make broader
520 inferences regarding peatland microforms in general. The SfM technique provides very
521 high resolution and accurate DEMs relatively quickly and easily. For studies which focus
522 on processes which are correlated with microtopographic position, a DEM or DSM
523 derived from ground- or drone-based imagery provides valuable information on
524 microtopographic variability and structure which can help inform plot selection, be used
525 for upscaling results, and quantify well defined morphometric and topographic variables
526 to aid in study inter-comparisons. Conversely, height measurements (e.g. using a dGPS



527 or other survey method) along a transect of at least 100 m with measurements taken at
528 an interval of less than 1 m provides sufficient information to describe a number of
529 peatland morphometric properties (e.g. hypsometry, roughness, fractal dimension, etc.).

530

531 Our study highlights the need to critically assess sampling approaches in peatland
532 ecosystem science where we show that a strict hummock-hollow classification tends to
533 under-sample intermediate topographic positions. While the discretization of peatland
534 ecosystems into microtopographic units has facilitated the understanding of peatland
535 processes in the context of species niche partitioning and their covariates such as water
536 table position, we now have techniques to better quantify variability with relative ease.
537 Consequently, techniques such as SfM enable us to consider peatland ecosystem
538 processes as part of a continuum. We must recognize that our conceptualizations, while
539 perhaps representing necessary simplifications, ought to be scrutinized to ensure that
540 elements of peatland complexity are not omitted. By considering microtopography
541 explicitly, we may be better able to understand how ecosystem complexity subsumed
542 within current microtopographic classifications might represent an important
543 unquantified confounding variable which limits our ability to adequately resolve and thus
544 understand certain peatland processes.

545

546 **DATA AVAILABILITY**

547 The post-processed point clouds used to generate digital elevation models which were
548 analysed in this study are available online at: [File are currently uploaded to a project



549 folder on Zenodo. Final publishing and assignment of DOI will be completed after review,
550 where additional material may be added based on recommendation(s) from reviewers].

551

552 **ACKNOWLEDGEMENTS**

553 We would like to thank James Sherwood and Paul Morris for valuable conversations
554 regarding the feasibility of this study and early discussions regarding research design.

555 We thank Lorna Harris for comments on an earlier draft of this manuscript. We also
556 thank Tom Ulanowski for data collection for the James Bay site, Rebekah Ingram and
557 Kristyn Mayner for data collection at the Red Earth Creek site, Mandy MacDougall,
558 Alanna Smolarz and Alex Furukawa for assistance with the Nobel data collection and
559 analysis, and to Lee Slater for data collection in Maine. This research was supported by
560 a NSERC Discovery Grant and NSERC Discovery Accelerator Supplement to JMW.

561



562 **REFERENCES**

563 Andrus, R., Wagner, D., and Titus, J.: Vertical zonation of *Sphagnum* mosses along
564 hummock-hollow gradients, *Can. J. Bot.*, 61, 3128-3139, doi:10.1139/b83-352, 1983.

565 Belyea, L. R., and Baird, A. J.: Beyond “the limits to peat bog growth”: Cross-scale
566 feedback in peatland development, *Ecol. Monogr.*, 76, 299–322, doi: 10.1890/0012-
567 9615(2006)076[0299:BTLTPB]2.0.CO;2, 2006.

568 Belyea, L. R., and Clymo, R. S.: Do hollows control the rate of peat bog growth.
569 *Patterned mires and mire pools*, 55-65, 1998.

570 Belyea, L. R., and Clymo, R. S.: Feedback control of the rate of peat formation. *Proc. of*
571 *the Royal Soc. London B: Biol. Sci.*, 268, 1315-1321, doi:10.1098/rspb.2001.1665,
572 2001.

573 Belyea, L. R., and Malmer, N.: Carbon sequestration in peatland: Patterns and
574 mechanisms of response to climate change, *Glob. Chang. Biol.* 10, 1043–1052,
575 doi.org/10.1111/j.1529-8817.2003.00783.x, 2004.

576 Benschoter, B. W., Wieder, R. K., and Vitt, D. H.: Linking microtopography with post-fire
577 succession in bogs, *J. Veg. Sci.*, 16, 453–460, doi:10.1111/j.1654-
578 1103.2005.tb02385.x, 2005.

579 Blodau, C., Basiliko, N., and Moore, T. R.: Carbon turnover in peatland mesocosms
580 exposed to different water table levels, *Biogeochem.*, 67, 331-351,
581 doi:10.1023/B:BIOG.0000015788.30164.e2, 2004.

582 Brown, M., and Lowe, D. G.: Unsupervised 3D object recognition and reconstruction in



- 583 unordered datasets. Fifth International Conference on 3-D Digital Imaging and
584 Modeling, 56-63, doi:10.1109/3DIM.2005.81, 2005.
- 585 Bruland, G. L., and Richardson, C. J.: Hydrologic, edaphic, and vegetative responses to
586 microtopographic reestablishment in a restored wetland, *Rest. Ecol.*, 13, 515-523,
587 doi:10.1111/j.1526-100X.2005.00064.x, 2005.
- 588 Bubier, J. L., Moore, T. R., and Roulet, N. T.: Methane emissions from wetlands in the
589 midboreal region of Northern Ontario, Canada, *Ecol.*, 74, 2240-2254, doi:
590 10.2307/1939577, 1993.
- 591 Campbell, D. R., Duthie, H. C., and Warner, B. G.: Post-glacial development of a kettle-
592 hole peatland in southern Ontario, *Ecosci.*, 4, 404-418,
593 doi:10.1080/11956860.1997.11682419, 2007.
- 594 Crill, P. M., Bartlett, K. B., Harriss, R. C., Gorham, E., Verry, E. S., Sebacher, D. I.,
595 Madzar, L., and Sanner, W.: Methane flux from Minnesota peatlands, *Global*
596 *Biogeochem. Cycles*, 2, 371-384, doi:10.1029/GB002i004p00371, 1988.
- 597 De Baets, S., van de Weg, M. J., Lewis, R., Steinberg, N., Meersmans, J., Quine, T. A.,
598 Shaver, G. R., and Hartley, I. P.: Investigating the controls on soil organic matter
599 decomposition in tussock tundra soil and permafrost after fire, *Soil Biol. Biochem.*, 99,
600 108-116, doi: 10.1016/j.soilbio.2016.04.020, 2016.
- 601 Dimitrov, D. D., Grant, R. F., Lafleur, P. M., and Humphreys, E. R.: Modeling peat
602 thermal regime of an ombrotrophic peatland with hummock–hollow microtopography,
603 *Soil Sci. Soc. Am. J.*, 74, 1406-1425, doi:10.2136/sssaj2009.0288, 2010.



- 604 Eppinga, M., Rietkerk, M., Borren, W., Lapshina, E. D., Bleuten, W., and Wassen, M. J.:
605 Regular surface patterning of peatlands: Confronting theory with field data,
606 *Ecosystems*, 11, 520–536, doi:10.1007/s10021-008-9138-z, 2008.
- 607 Forbrich, I., Kutzbach, L., Wille, C., Becker, T., Wu, J., and Wilmking, M.: Cross-
608 evaluation of measurements of peatland methane emissions on microform and
609 ecosystem scale using high-resolution landcover classification and source weight
610 modelling, *Ag. For. Met.*, 151, 864-874, doi:10.1016/j.agrformet.2011.02.006, 2011.
- 611 Frenzel, P., and Karofeld, E.: CH₄ emission from a hollow-ridge complex in a raised bog:
612 The role of CH₄ production and oxidation, *Biogeochem.*, 51, 91-112,
613 doi:10.1023/A:1006351118347, 2000.
- 614 Granath, G., Wiedermann, M. M., and Strengbom, J.: Physiological responses to
615 nitrogen and sulphur addition and raised temperature in *Sphagnum balticum*,
616 *Oecologia*, 161, 481-490, doi:10.1007/s00442-009-1406-x, 2009.
- 617 Griffis, T. J., Rouse, W. R., and Waddington, J. M.: Scaling net ecosystem exchange
618 from the community to the landscape level at a subarctic fen, *Glob. Change Biol.*, 6,
619 459-473, doi: 10.1046/j.1365-2486.2000.00330.x, 2000.
- 620 Harley, P. C., Tenhunen, J. D., Murray, K. J., and Beyers, J.: Irradiance and
621 temperature effects on photosynthesis of tussock tundra *Sphagnum* mosses from the
622 foothills of the Philip Smith Mountains, Alaska, *Oecologia*, 79(2), 251-259, doi:
623 10.1007/BF00388485, 1989.
- 624 Harris, A., and Baird, A. J., Microtopographic Drivers of Vegetation Patterning in Blanket



625 Peatlands Recovering from Erosion, *Ecosystems*, 1-20, doi: 10.1007/s10021-018-
626 0321-6, 2018.

627 Hayward, P. M., and Clymo, R. S.: Profiles of water content and pore size in Sphagnum
628 and peat, and their relation to peat bog ecology. *Proceedings of the Royal Society of*
629 *London. Series B. Biological Sciences*, 215(1200), 299-325, 1982.

630 Hodgkins, S. B., Richardson, C. J., Dommain, R., Wang, H., Glaser, P. H., Verbeke, B.,
631 Winkler, R. B., Cobb, A. R., Rich, V. I., Missilmani, M., Flanagan, N., Ho, M., Hoyt, A.
632 M., Harvey, C. F., Vining, S. R., Hough, M. A., Moore, T. R., Richard, P. J. H., De La
633 Cruz, F. B., Toufaily, J., Hamdan, R., Cooper, W. T., and Chanton, J. P.: Tropical
634 peatland carbon storage linked to global latitudinal trends in peat recalcitrance.
635 *Nature Comm.*, 9, 3640, doi: 10.1038/s41467-018-06050-2, 2018.

636 Humphreys, E. R., Lafleur, P. M., Flanagan, L. B., Hedstrom, N., Syed, K. H., Glenn, A.
637 J., and Granger, R.: Summer carbon dioxide and water vapor fluxes across a range
638 of northern peatlands, *J. Geophys. Res.*, 111, G04011, doi:10.1029/2005JG000111,
639 2006.

640 Ise, T., Dunn, A. L., Wofsy, S. C., and Moorcroft, P. R.: High sensitivity of peat
641 decomposition to climate change through water-table feedback, *Nature Geosci.*, 1,
642 763-766, doi:10.1038/ngeo331, 2008.

643 Kettridge, N., and Baird, A. J.: Modelling soil temperatures in northern peatlands, *Eur. J.*
644 *Soil Sci.*, 59, 327–338, doi:2389.2007.01000.x, 2008.

645 Kettridge, N., and Baird, A.: Simulating the thermal behavior of northern peatlands with



646 a 3 - D microtopography, J. Geophys. Res.: Biogeosciences, 115, G03009, doi:
647 10.1029/2009JG001068, 2010.

648 Kettridge, N., and Waddington, J.M.: Towards quantifying the negative feedback
649 regulation of peatland evaporation to drought, Hydrological Processes, 28(11), 3728-
650 3740, doi: 10.1002/hyp.9898, 2014.

651 Kettridge, N., Comas, X., Baird, A., Slater, L., Strack, M., Thompson, D., Jol, H., and
652 Binley, A.: Ecohydrologically important subsurface structures in peatlands revealed
653 by ground-penetrating radar and complex conductivity surveys, J. Geophys. Res.,
654 113, G04030, doi:10.1029/2008JG000787, 2008.

655 Kettridge, N., Turetsky, M. R., Sherwood, J. H., Thompson, D. K., Miller, C. A.,
656 Benscoter, B. W., and Waddington, J. M.: Moderate drop in water table increases
657 peatland vulnerability to post-fire regime shift, Sci. Rep., 5, 8063,
658 doi:10.1038/srep08063, 2015.

659 Kumar, L., Skidmore, A. K. and Knowles, E.: Modelling topographic variation in solar
660 radiation in a GIS environment. International Journal of Geographical Information
661 Science, 11(5), 475-497, doi: 10.1080/136588197242266, 1997.

662 Lafleur, P. M., Roulet, N. T., Bubier, J. L., Frohling, S., and Moore, T. R.: Interannual
663 variability in the peatland-atmosphere carbon dioxide exchange at an ombrotrophic
664 bog. Glob. Biogeochem. Cycles, 17, 1036, doi:10.1029/2002GB001983, 2003.

665 Lafleur, P. M., Moore, T. R., Roulet, N. T., and Frohling, S.: Ecosystem respiration in a
666 cool temperate bog depends on peat temperature but not water table, Ecosystems, 8,



- 667 619-629, doi:10.1007/s10021-003-0131-2, 2005.
- 668 Laing, C. G., Shreeve, T. G., and Pearce, D. M. E.: Methane bubbles in surface peat
669 cores: in situ measurements, *Glob. Change Biol.*, 14, 916–924, doi:10.1111/j.1365-
670 2486.2007.01534, 2008.
- 671 Larsen, L. G., Eppinga, M. B., Passalacqua, P., Getz, W. M., Rose, K. M. and Liang, M.:
672 Appropriate complexity landscape modeling, *Earth Sci. Rev.*, 160, 111-130,
673 doi:10.1029/2008JG000787, 2016.
- 674 Loisel, J., Gallego-Sala, A. V., and Yu, Z. C.: Global-scale pattern of peatland
675 Sphagnum growth driven by photosynthetically active radiation and growing season
676 length, *Biogeosciences*, 9, 2737-2746, doi: 10.5194/bg-9-2737-2012, 2012.
- 677 Lowe, D. G.: Object recognition from local scale-invariant features. The proceedings of
678 the seventh IEEE international conference on Computer vision, 2, 1150-1157,
679 doi:10.1109/ICCV.1999.790410, 1999.
- 680 Lukenbach, M. C., Kettridge, N., Devito, K. J., Petrone, R. M., and Waddington, J. M.:
681 Hydrogeological controls on post-fire moss recovery in peatlands, *J. Hydrol.*, 530,
682 405-418, doi:10.1016/j.jhydrol.2015.09.075, 2015.
- 683 Maholtra, A., Roulet, N. T., Wilson, P., Giroux-Bougard, X., and Harris, L. I.:
684 Ecohydrological feedbacks in peatlands: an empirical test of the relationship among
685 vegetation, microtopography and water table, *Ecohydrol.*, 9, 1346-1357,
686 doi:1002/eco.1731, 2016.
- 687 MathWorks, Inc.: MATLAB, Version 8.5, MathWorks, Natick, Mass., 2015.



- 688 Mercer, J. J., and Westbrook, C. J.: Ultrahigh-resolution mapping of peatland microform
689 using ground-based structure from motion with multiview stereo, *J. Geophys. Res.*
690 *Biogeosci.*, 121, 2901-2916, doi:10.1002/2016JG003478, 2016.
- 691 Moore, T. R., and Roulet, N. T., and Waddington, J. M.: Uncertainty in predicting the
692 effect of climatic change on the carbon cycling of Canadian peatlands, *Clim. Change*,
693 40, 229-245, doi:10.1023/A:1005408719297, 1998.
- 694 Moore, P. A., Morris, P. J., and Waddington, J. M.: Multi-decadal water table
695 manipulation alters peatland hydraulic structure and moisture retention, *Hydrol. Proc.*,
696 29, 2970-2982, doi:10.1002/hyp.10416, 2015.
- 697 Moore, P. A., Lukenbach, M. C., Kettridge, N., Petrone, R. M., Devito, K. J. and
698 Waddington, J. M.: Peatland water repellency: Importance of soil water content, moss
699 species, and burn severity, *Journal of Hydrology*, 554, 656-665, doi:
700 10.1016/j.jhydrol.2017.09.036, 2017.
- 701 Moore, P. A., Smolarz, A. G., Markle, C. E., and Waddington, J. M.: Hydrological and
702 thermal properties of moss and lichen species on rock barrens: Implications for
703 turtle nesting habitat, *Ecohydrol.*, 12, e2057, doi:10.1002/eco.2057, 2019.
- 704 Moser, K., Ahn, C., and Noe, G.: Characterization of microtopography and its influence
705 on vegetation patterns in created wetlands, *Wetlands*, 27, 1081-1097, doi:
706 10.1672/0277-5212(2007)27[1081:COMAI]2.0.CO;2, 2007.
- 707 Nijp, J. J., Limpens, J., Sjoerd, K. M., van der Zee, E. A. T. M., Berendse, F., and
708 Robroek, B. J. M.: Can frequent precipitation moderate the impact of drought on



- 709 peatmoss carbon uptake in northern peatlands? *New Phytol.*, 203, 70-80,
710 doi:10.1111/nph.12792, 2014.
- 711 Nungesser, M. K.: Modelling microtopography in boreal peatlands: hummocks and
712 hollows, *Ecol. Mod.*, 165, 175-207, doi:10.1016/S0304-3800(03)00067-X, 2003.
- 713 Pedrotti, E., Rydin, H., Ingmar, T., Hytteborn, H., Turunen, P., and Granath, G.:
714 Fine-scale dynamics and community stability in boreal peatlands: revisiting a
715 fen and a bog in Sweden after 50 years, *Ecosphere*, 5, 133, doi: 10.1890/ES14-
716 00202.1, 2014.
- 717 Peichl, M., Öquist, M., Löfvenius, M.O., Ilstedt, U., Sagerfors, J., Grelle, A., Lindroth, A.,
718 and Nilsson, M.B.: A 12-year record reveals pre-growing season temperature and
719 water table level threshold effects on the net carbon dioxide exchange in a boreal fen,
720 *Env. Res. Lett.*, 9, 055006, doi: 10.1088/1748-9326/9/5/055006, 2014.
- 721 Pelletier, L., Garneau, M., and Moore, T. R.: Variation in CO₂ exchange over three
722 summers at microform scale in a boreal bog, Eastmain region, Québec, Canada, *J.*
723 *Geophys. Res.*, 116, G03019, doi:10.1029/2011JG001657, 2011.
- 724 Petrone, R. M., Solondz, D. S., Macrae, M. L., Gignac, D., and Devito, K. J.:
725 Microtopographical and canopy cover controls on moss carbon dioxide exchange in a
726 western Boreal Plain peatland. *Ecohydrol.*, 4, 115-129, doi:10.1002/eco.139, 2011.
- 727 Rahman, M. M., McDermid, G. J., Strack, M., and Lovitt, J.: A new method to map
728 groundwater table in peatlands using unmanned aerial vehicles, *Rem. Sens.*, 9,
729 1057, doi: 10.3390/rs9101057 , 2017.



730 Regina, K., Nykänen, H., Silvola, J., and Martikainen, P. J.: Fluxes of nitrous oxide from
731 boreal peatlands as affected by peatland type, water table level and nitrification
732 capacity, *Biogeochem.*, 35, 401-418, doi:10.1007/BF02183033, 1996.

733 Rydin, H.: Effect of water level on desiccation of *Sphagnum* in relation to surrounding
734 Sphagna, *Oikos*, 45(3), 374-379, doi: 10.2307/3565573, 1985.

735 Rydin, H., and McDonald, A. J. S.: Tolerance of *Sphagnum* to water level, *J. Bryol.*, 13,
736 571-578, doi:10.1179/jbr.1985.13.4.571., 1985.

737 Shannon, R. D., and White, J. R.: A three-year study of controls on methane emissions
738 from two Michigan peatlands, *Biogeochem.*, 27, 35-60, doi:10.1007/BF00002570,
739 1994.

740 Sonnentag, O., Chen, J. M., Roulet, R. T., Ju, W., and Govind, A.: Spatially explicit
741 simulation of peatland hydrology and carbon dioxide exchange: Influence of
742 mesoscale topography, *J. Geophys. Res.*, 113, G02005, doi:10.1029/2007JG000605,
743 2008.

744 Strack, M., and Price, J.S.: Moisture controls on carbon dioxide dynamics of peat -
745 *Sphagnum* monoliths. *Ecohydrology*, 2(1), 34-41, doi: 10.1002/eco.36, 2009

746 Turetsky, M., Wieder, K., Halsey, L., and Vitt, D.: Current disturbance and the
747 diminishing peatland carbon sink, *Geophys. Res. Lett.*, 29, 1526,
748 doi:10.1029/2001GL014000, 2002.

749 Turetsky, M. R., Kotowska, A., Bubier, J., Dise, N. B., Crill, P., Hornibrook, E. R. C.,
750 Minkinen, K., Moore, T. R., Myers-Smith, I. H., Nykänen, H., Olefeldt, D., Rinne, J.,



- 751 Saarnio, S., Shurpali, N., Tuittila, E-S., Waddington, J. M., White, J. R., Wickland, K.
752 P., and Wilmking, M.: A synthesis of methane emissions from 71 northern, temperate,
753 and subtropical wetlands, *Glob. Change Biol.*, 20, 2183-2197, doi:10.1111/gcb.12580,
754 2014.
- 755 Ulanowski, T. A., and Branfireun, B. A.: Small-scale variability in peatland pore-water
756 biogeochemistry, Hudson Bay Lowland, Canada, *Sci. Tot. Environ.*, 454-455, 211-
757 218, doi:10.1016/j.scitotenv.2013.02.087, 2013.
- 758 Waddington, J. M., and Roulet, N. T.: Atmosphere-wetland carbon exchanges: Scale
759 dependency of CO₂ and CH₄ exchange on the developmental topography of a
760 peatland, *Global Biogeochem. Cycles*, 10, 233-245, doi:10.1029/95GB03871, 1996.
- 761 Waddington, J. M., Harrison, K., Kellner, E., and Baird, A. J.: Effect of atmospheric
762 pressure and temperature on entrapped gas content in peat, *Hydrol. Proc.*, 23, 2970-
763 2980, doi: 10.1002/hyp.7412, 2009.
- 764 Waddington, J. M., Morris, P. J., Kettridge, N., Granath, G., Thompson, D. K., and
765 Moore, P. A.: Hydrological feedbacks in northern peatlands, *Ecohydrology*, 8, 113-
766 127, doi:10.1002/eco.1493, 2015.
- 767 Wieder, R. K., Scott, K. D., Kamminga, K, Vile, M. A., Vitt, D. H., Bone, T., Xu, B. I.,
768 Benschoter, B. W., and Bhatti, J. S.: Postfire carbon balance in boreal bogs of Alberta,
769 Canada, *Glob. Change Biol.*, 15, 63-81, doi:10.1111/j.1365-2486.2008.01756.x, 2009.
- 770 Williams, T. G., and Flanagan, L. B.: Measuring and modelling environmental influences
771 on photosynthetic gas exchange in *Sphagnum* and *Pleurozium*. *Plant, Cell &*



- 772 Environment, 21(6), 555-564, doi: 10.1046/j.1365-3040.1998.00292.x,1998.
- 773 Wu, C.: VisualSFM: A visual structure from motion system, 2011.
- 774 Yu, Z. C.: Northern peatland carbon stocks and dynamics: a review, Biogeosci., 9,
775 4071–4085, doi: 10.5194/bg-9-4071-2012, 2012.
- 776 Yu, Z., Beilman, D. W., and Jones, M. C.: Sensitivity of northern peatland carbon
777 dynamics to Holocene climate change, Carbon cycling in northern peatlands, pages
778 55-69, doi:10.1029/2008GM000822, 2009.



779 **Table 1: Summary information on sample locations and SfM reconstructions of**
 780 **microtopographic variation for target areas for randomly and qualitatively chosen**
 781 **plot locations within a site.**
 782

Location	Plot Name	Lat. (°N)	Lon. (°W)	Plot Area (m ²)	Number of Images Used	Point Cloud Density (m ⁻²)
<i>Random</i>						
Nobel, ON ¹	Alpha	45.434	80.081	4.6	47	6.04 × 10 ⁴
--	Beta	--	--	3.8	41	7.83 × 10 ⁴
--	Gamma	--	--	4.1	44	6.68 × 10 ⁴
--	Epsilon	--	--	5.2	53	8.38 × 10 ⁴
--	Zeta	--	--	6.12	66	1.60 × 10 ⁵
--	Eta	--	--	5.74	60	1.42 × 10 ⁵
--	Iota	--	--	5.66	49	3.23 × 10 ⁴
--	Kappa	--	--	5.53	66	1.77 × 10 ⁵
--	Theta	--	--	5.48	59	1.38 × 10 ⁵
--	Lambda	--	--	8.2	61	1.18 × 10 ⁵
<i>Qualitative</i>						
Caribou Bog, MN ²	Maine	44.83	68.75	10.1	79	3.75 × 10 ⁴
James Bay, ON ³	JamesBay	52.846	83.930	7.6	82	1.97 × 10 ⁵
Ottawa, ON	Limerick	44.877	75.609	9.0	282	5.94 × 10 ⁵
Puslinch, ON ⁴	Puslinch	43.407	80.264	6.45	109	1.12 × 10 ⁵
Rödmossen, SWE ⁵	Sweden	60.013	-17.355	10.6	105	4.71 × 10 ⁴
Seney, MI ⁶	WET	46.190	86.019	7.7	135	1.12 × 10 ⁵
Seney, MI ⁶	INT	46.192	86.019	7.0	109	9.44 × 10 ⁴
Seney, MI ⁶	DRY	46.186	86.015	7.3	62	8.89 × 10 ⁴
Nobel, ON ¹	Lambda	45.434	80.081	8.2	61	1.18 × 10 ⁴

783 For detailed site information see the following studies: 1. Moore et al., (2019); 2.
 784 Kettridge et al. (2008); 3. Ulanowski and Branfireuen (2013); 4. Campbell et al. (1997);
 785 5. Granath et al. (2009); 6. Moore et al. (2015).



786 **Table 2: Estimated parameters for one-, two-, or three-member Gaussian mixture model (GMM) fit to DEM**
 787 **elevations. Results are presented for the GMM which minimizes AIC. Plots are separated into those chosen at**
 788 **random versus qualitatively at their respective site.**
 789

Location	Plot Name	1 st distribution			2 nd distribution			3 rd distribution		
		Mean	SD	Scale	Mean	SD	Scale	Mean	SD	Scale
<i>Random</i>										
Nobel, ON	Alpha	0.11	0.03	0.23	0.20	0.03	0.36	0.28	0.06	0.41
--	Beta	0.13	0.04	0.37	0.18	0.03	0.53	0.29	0.04	0.10
--	Epsilon	0.07	0.02	0.06	0.18	0.05	0.30	0.31	0.05	0.64
--	Gamma	0.19	0.08	0.23	0.26	0.04	0.59	0.44	0.06	0.18
--	Zeta	0.11	0.03	1	—	—	—	—	—	—
--	Eta	0.13	0.04	0.82	0.25	0.05	0.18	—	—	—
--	Iota	0.11	0.03	0.24	0.19	0.06	0.76	—	—	—
--	Kappa	0.11	0.04	0.23	0.23	0.06	0.60	0.42	0.05	0.06
--	Theta	0.16	0.03	0.84	0.25	0.04	0.16	—	—	—
<i>Qualitative</i>										
Caribou Bog, ME	Maine	0.07	0.02	0.15	0.16	0.02	0.55	0.28	0.07	0.30
James Bay, ON	JamesBay	0.17	0.08	1	—	—	—	—	—	—
Ottawa, ON	Limerick	0.08	0.02	0.38	0.15	0.05	0.62	—	—	—
Puslinch, ON	Puslinch	0.14	0.053	1	—	—	—	—	—	—
Rödmosse	Sweden	0.17	0.05	0.87	0.36	0.04	0.13	—	—	—
Seney, MI	WET	0.23	0.08	0.59	0.36	0.05	0.25	0.44	0.03	0.16
Seney, MI	INT	0.25	0.07	0.51	0.45	0.06	0.40	0.53	0.02	0.09
Seney, MI	DRY	0.08	0.03	0.05	0.21	0.04	0.45	0.34	0.05	0.50
Nobel, ON	Lambda	0.05	0.02	0.46	0.20	0.08	0.54	—	—	—



790 **LIST OF FIGURES:**

791 Figure 1: Relation between standard deviation of microtopographic variation based on
792 total sample area for the Red Earth Creek site based on fifty ~ 3.5 m² plots. The grey
793 shaded area represents the 2.5 and 97.5 percentile of standard deviation from the
794 Monte Carlo resampling procedure.

795

796 Figure 2: Absolute (solid lines) and cumulative (dashed lines) power spectral density of
797 height along a 300 m transect for the Red Earth Creek, AB (red) and Nobel, ON (black)
798 sites.

799

800 Figure 3: Relative frequency distribution of height in plots where a perceived
801 representative hummock and adjacent hollow was subjectively chosen for a given site.
802 Relative height distributions are shown for the entire plot (A) and for a hummock and
803 hollow subplot (B) whose area corresponds to the size of a large flux measurement
804 chamber. Elevations are referenced to the lowest point of the reconstructed surface and
805 set to zero.

806

807 Figure 4: Relative frequency distribution of height in plots with randomly chosen
808 locations within a site containing a perceived hummock and adjacent hollow. Relative
809 height distributions are shown for the entire plot (A) and for a hummock and hollow
810 subplot (B) whose area corresponds to the size of a large flux measurement chamber.
811 Elevations are referenced to the lowest point of the reconstructed surface and set to
812 zero.



813

814 Figure 5: Radially averaged power spectral density for randomly– (left panel) and
815 qualitatively– (right panel) chosen plots representing the change in elevation variability
816 with length scale. The slope between the power spectral density and wavevector
817 ($2\pi/\text{wavelength}$) in log-log space corresponds with the Hurst exponent (H), where
818 slope = $-2(H+1)$; and is related to the fractal dimension as $3-H$.

819

820 Figure 6: Weibull probability density function of slope derived from surface normal of a
821 planar fit to elevation in a moving 0.03 m x 0.03 m window for all DEMs. Panels (a) and
822 (b) separate the randomly and qualitatively chosen plots, respectively.

823

824 Figure 7: Variation in potential solar insolation relative to a flat surface based on aspect
825 (a) and slope (b). Boxplots shows median and inter-quartile range, with outliers shown
826 as dots. Insolation as a function of slope has been bin averaged per cardinal direction,
827 where each point represents 100 data points. Slope and aspect data are for the Seney,
828 WET plot.

829

830 Figure 8: Mean potential net photosynthesis (NPP) for three microtopographic classes
831 (i.e. high-hummock, low-hummock, and lawn/hollow — see supplementary figure 1)
832 derived from spatially explicit elevation data for random (a,c) and qualitatively chosen
833 (b,d) plots. NPP-WC and WC-WTD relations are based on separate parameterization
834 for each microtopography class (see supplementary figure 2).

835

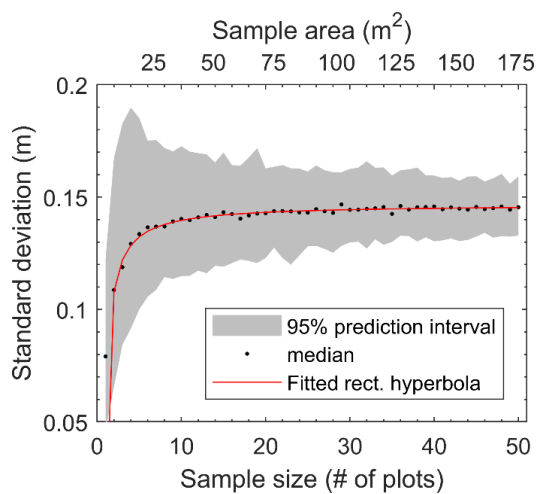


836 Figure 9: Difference in maximum potential net photosynthesis (NPP_{pot}) between models
837 using the measured distribution of elevation over the entire SfM-derived DEM and the
838 measured distribution within hummock-hollow subplots. NPP_{pot} is modelled using
839 separate parameterization (Figure S2) for each microtopography class (a), as well as a
840 uniform (low-hummock) parameterization across microtopography classes (b).

841



842 [Figure 1]

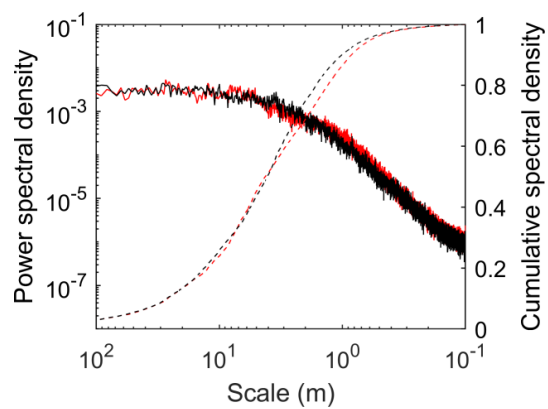


843

844

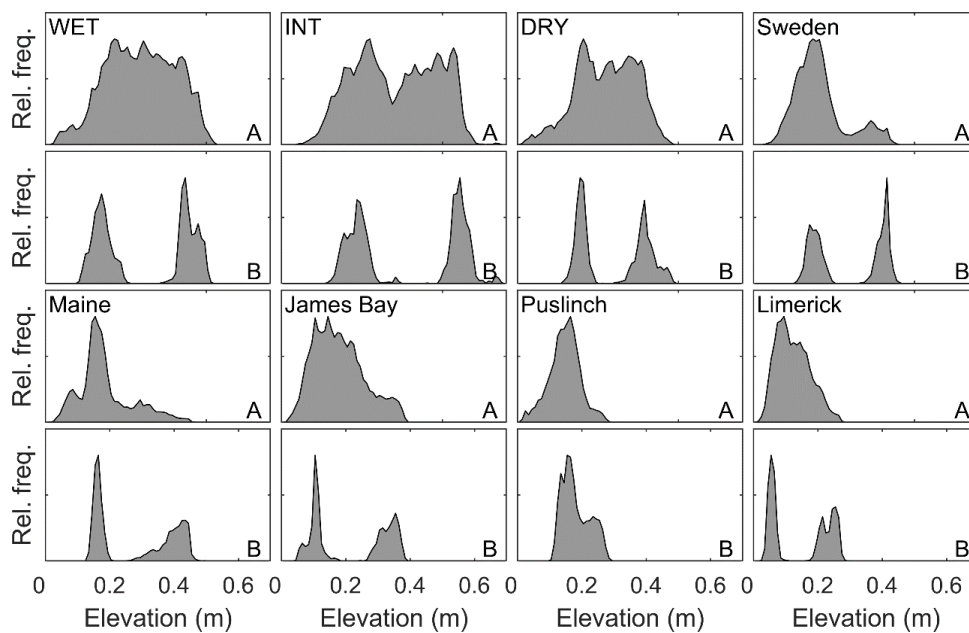


845 [Figure 2]





848 [Figure 3]

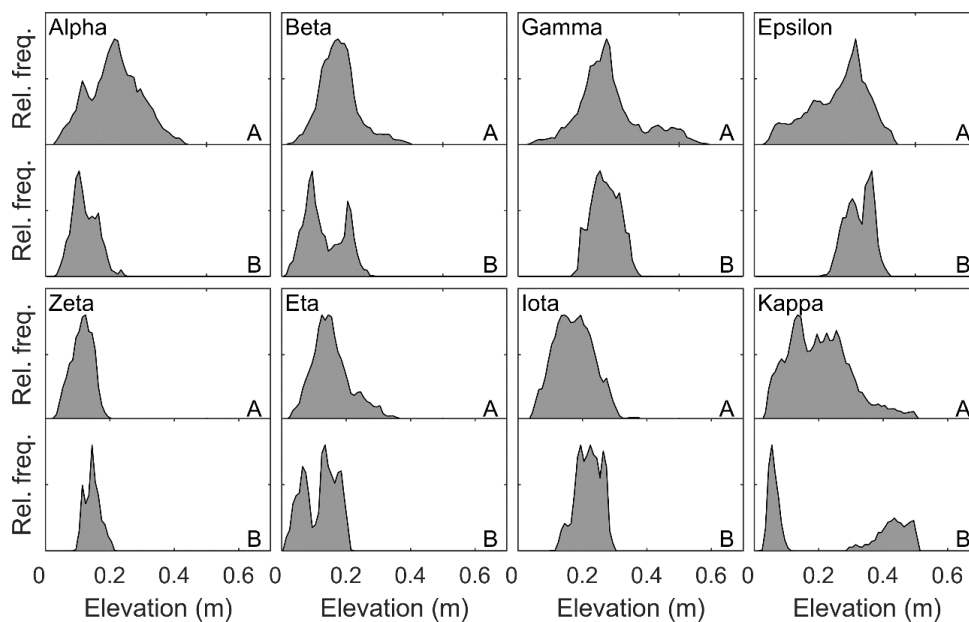


849

850



851 [Figure 4]

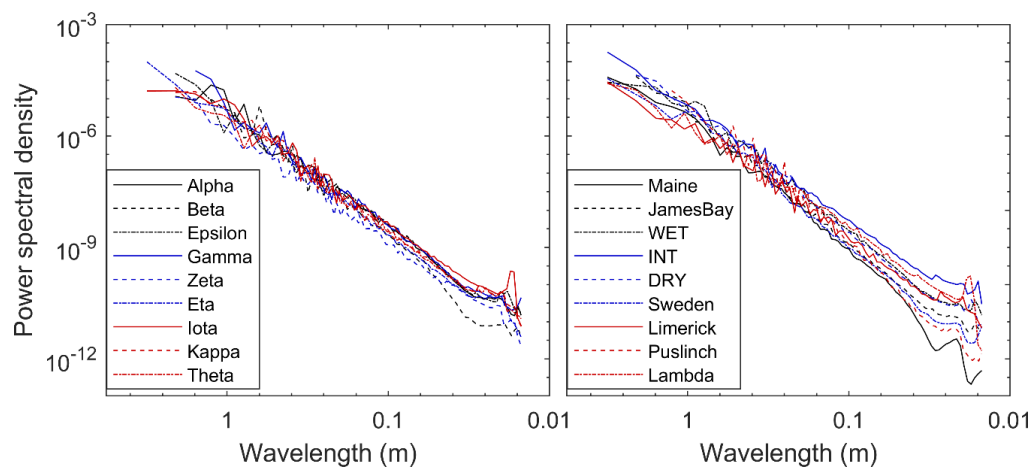


852

853



854 [Figure 5]

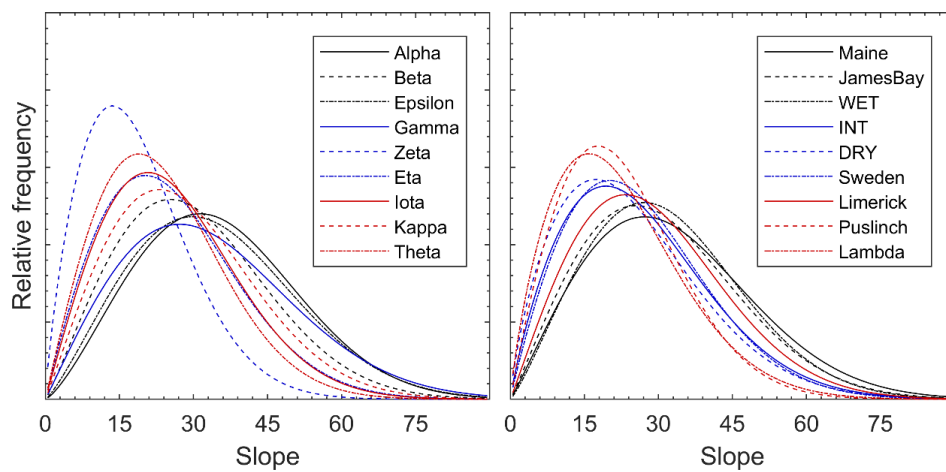


855

856



857 [Figure 6]



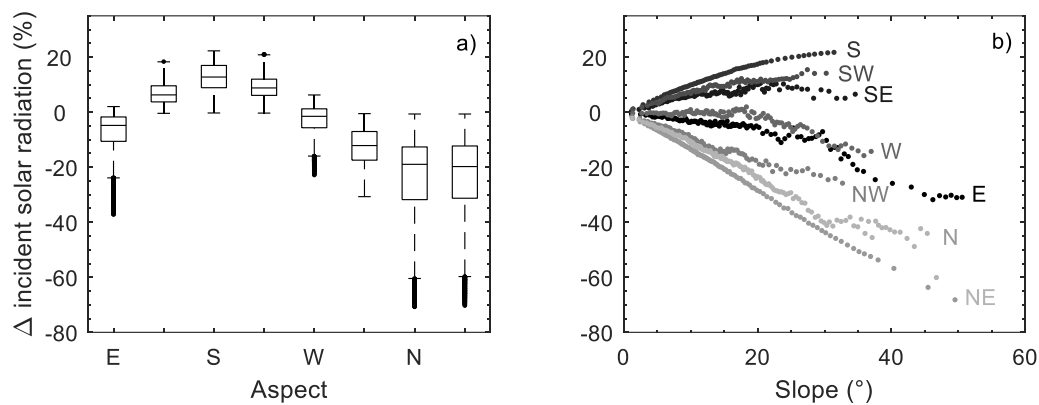
858

859

860



861 [Figure 7]



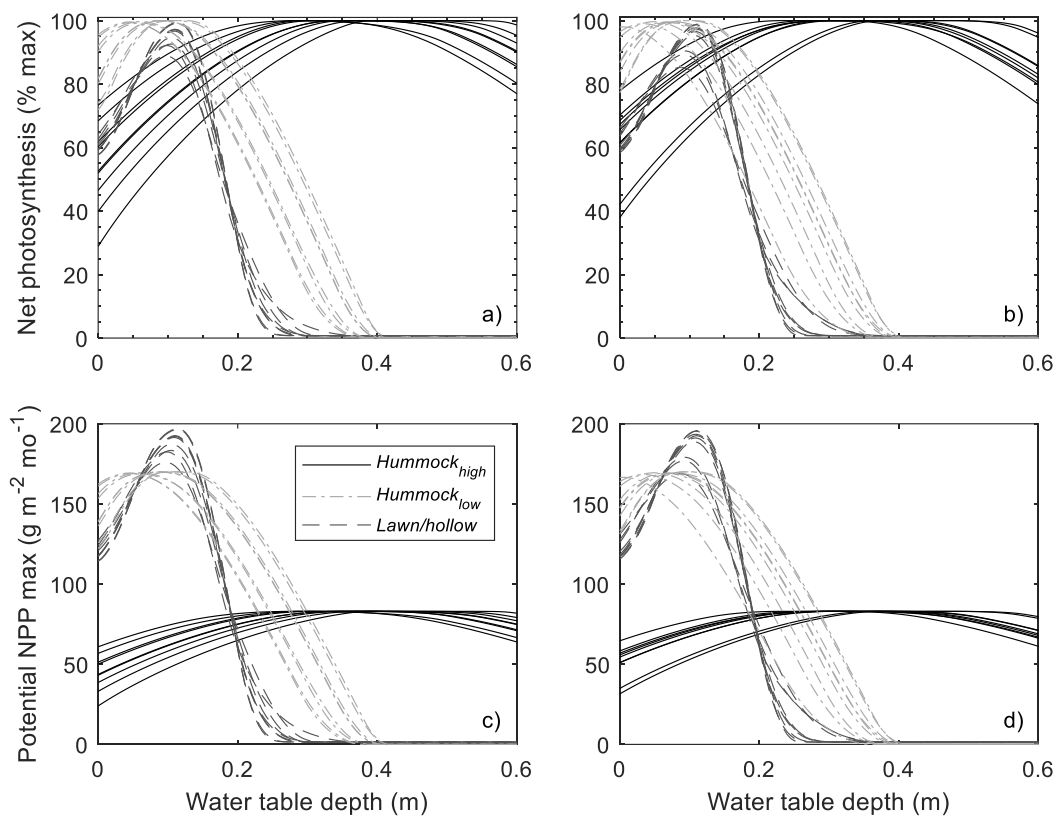
862

863

864



865 [Figure 8]



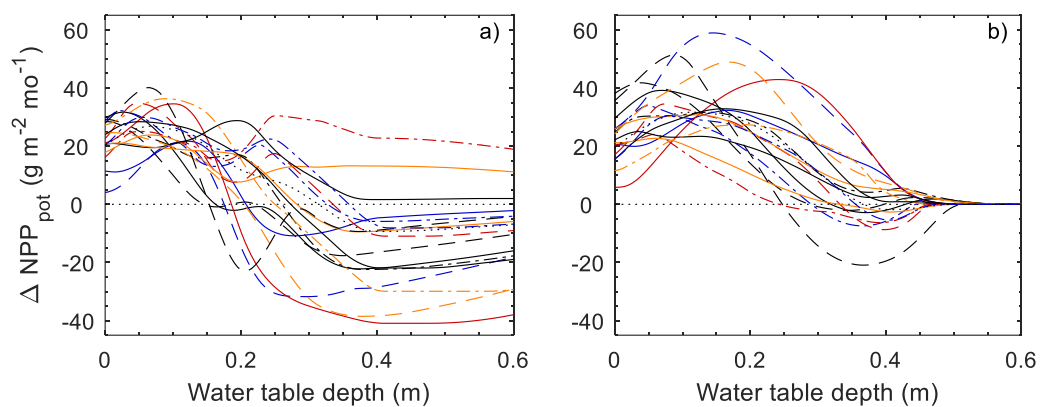
866

867

868



869 [Figure 9]



870

871